Paper No.
08380

NACE INTERNATIONAL CORROSION 2008 CONFERENCE & EXPO

GALVANIC BEHAVIOR OF ALUMINIZED STEEL TYPE 2 WITH COATING BREAKS IN WATERS OF VARYING SCALING TENDENCIES

Leonardo Caseres
Mechanical & Materials Engineering Division, Southwest Research Institute
San Antonio, TX 78238, USA

Alberto A. Sagüés
Department of Civil and Environmental Engineering, University of South Florida
Tampa, FL 33620, USA

ABSTRACT

Aluminized steel Type 2 is produced as a carbon steel sheet hot dip coated on both sides with commercially pure aluminum, forming a layered Al/Al-Fe coating that provides corrosion protection through low corrosion rates of the sound outer aluminum when it is passive. However, if the aluminized coating is partially disrupted exposing the underlying steel, accelerated damage by galvanic corrosion of the aluminized coating and/or the exposed steel may take place. To examine this condition, the impedance behavior of aluminized steel Type 2 with coating breaks of various sizes was studied in waters of controlled varying scaling tendencies containing different amounts of Ca^{+2}, HCO_3^-, and Cl^- ions at room temperature. Initial findings show accelerated corrosion at the exposed steel in mild solutions early in the test, indicative of poor galvanic protection by the coating. However, enhanced galvanic protection by the surrounding aluminized coating was noted later on in the test. Impedance measurements confirmed that corrosion of the aluminized coating was in progress then, resulting in larger protective currents.

Keywords: aluminized steel, galvanic corrosion, coating break, electrochemical impedance

INTRODUCTION

Aluminized steel Type 2 is produced by hot-dipping a low carbon steel sheet in a commercially pure aluminum bath. The end product has a ~40 µm thick coating consisting of a thicker outer layer of nearly pure aluminum and a thinner intermediate layer of aluminum-iron alloy in contact with the steel substrate. The outer layer contains significant amounts of Fe, leading to the formation of micrometer-scale Fe-rich constituent inclusions, e.g. $FeAl_3$ and

Fe_2Al_5, in the aluminum matrix[1-3]. The main purpose of the aluminized metallic coating is to protect the underlying steel against corrosion due to its excellent intrinsic corrosion resistance compared to other metallic coatings. Aluminized steel Type 2 is commonly used for drainage culvert pipe applications designed to operate for long service lives (e.g. 75 years and beyond) so that extremely low corrosion rates are desirable[4]. If the aluminized coating is partially disrupted exposing the underlying steel, the service life of the aluminized steel component may be considerably shortened by corrosion of the steel, and/or by accelerated corrosion of the aluminized coating depending on the extent of galvanic action present.

Past experimental work has been limited to study the galvanic corrosion performance of aluminized steel Type 2 exposed to various atmospheric environments and aggressive media. There is experimental evidence that aluminized coating exposed to aggressive environments has the ability to act as a sacrificial anode galvanically protecting the exposed steel. For instance, Legault and Pearson[5] evaluated the atmospheric corrosion of aluminized steel Type 2 with exposed steel at the uncoated cut edges placed in a marine atmospheric environment, reporting that iron-rust stains from exposed cut edges were not observed. Instead, a uniform white corrosion product developed on the aluminized coating indicative of appreciable galvanic protection to the exposed steel. Similar observations were reported by Townsend and Zoccola[6], and later by Townsend and Borzillo[7]. Creus[8] found that aluminized steel when coupled to steel of 3 cm^2 surface area immersed in 0.5 M NaCl solution delivered a generous protective galvanic current of ~300 $\mu A/cm^2$ shortly after exposure. However, in mild atmospheric environments, e.g. rural and industrial, rust formation was noted at the exposed steel whereas the aluminized coating remained passive over the entire exposure time, providing little to no galvanic protection[9].

This work aims at determining the galvanic behavior of mechanically distressed aluminized steel Type 2, with underlying steel exposed at the coating break. The samples were immersed in waters of varying scaling tendencies with moderate chloride content, of compositions relevant to those found in Florida natural waters. These conditions are of interest as environmental aggressivity may be sufficient to cause significant corrosion of the exposed steel, but not enough to promote adequate galvanic current from the aluminized coating. Of concern is to determine the amount of current delivered by the coating when coupled to small areas of exposed steel, and the mechanisms associated with the galvanic corrosion processes relevant to better forecasting durability in critical highway applications.

EXPERIMENTAL PROCEDURE

Aluminized steel Type 2 was manufactured according to ASTM A929, from low carbon steel (Table 1) coils rolled to 16 gage (~1.59 mm thick). The microstructure (Figure 1) had a pearlite-free ferrite substrate with regular grains. The aluminized coating layer included a partly columnar inner layer ~10-15 μm thick, of approximate composition Fe_2Al_5[10] as determined by scanning electron microscopy (SEM) with energy dispersive x-ray analysis (EDS), and an outer layer ~20-30 μm thick. The composition of the outer gray layer matrix and the small gray lighter features were predominantly Al with ~2.4 wt% Fe and 6-11 wt% Fe respectively. The light features resemble Fe-rich precipitates identified elsewhere[11].

Test specimens with a circular 95 cm^2 nominal surface area exposed to solution were cut out from the as-received flat aluminized steel sheet. Coating breaks 2 cm (LCB specimens)

and 0.2 cm (SCB specimens) diameter and 300 μm deep were machined in the center of one of the specimen faces exposing the underlying steel. A 500 mL three-electrode test cell configuration similar to that described earlier[12] was used. Additional experiments (Figure 2) exposed together an as-received unblemished aluminized steel specimen of 95 cm^2 nominal surface area placed at the bottom of the cell and a separate but normally interconnected (except during impedance and galvanic measurements) 3 cm^2 nominal surface area steel component, made by mechanically stripping the aluminized coating and wet grounding to a 320-grit surface finish. The aluminized coating/exposed steel area ratio matched that of the LCB specimens. The test cell thus constructed served to monitor galvanic currents between the unblemished aluminized steel and the steel components as well as the electrochemical impedance of the individual macrocell components.

The test solutions (Table 2) were prepared from de-carbonated de-ionized water of resistivity higher than 10^6 Ω-cm, and corresponded to a carbonate precipitating condition (solution P combining reagent grade $NaHCO_3$, HCl, and $Ca(OH)_2$), a mildly alkaline but non-precipitating condition (solution NP made with $NaHCO_3$, NaCl, and HCl), a neutral pH of non carbonate precipitating and negligible alkalinity condition (solution C made with NaOH and NaCl), and a simulated ocean water (solution SW) prepared according to ASTM D1141-90 standard procedure. Test solutions C and NP had a Langelier Saturation Index LSI = -5.9 and -0.6, respectively. Test solutions P and SW had LSI = +1.5 and +0.4, respectively, in agreement with the formation of a thin powdery layer precipitate of $CaCO_3$ in both solutions shortly after preparation. The test solutions in the test cells were quiescent and naturally aerated through a small opening. The relatively small electrolyte volume/total specimen area ratio was intended to be representative of, for instance, worst-case culvert pipe conditions with stagnant water on the pipe invert, or of occluded conditions for pore water on the soil side of a pipe.

The immersion tests were conducted in duplicate and in some cases in triplicate for up to ~3,500 hr at 22±2˚C. Solution pH, conductivity, and open circuit potential (E_{OC}) reported in the SCE scale were monitored periodically. To map the E_{OC} profile with radius a Luggin capillary placed at ~1 mm from the metal surface was manually scanned over the LCB specimen surface exposed to solutions P and NP. Electrochemical impedance spectroscopy (EIS) measurements were obtained at the E_{OC} in the frequency range from 100 kHz to 1 mHz using sinusoidal signals of 10 mV rms amplitude. Galvanic currents were measured with a 0.1 Ω resistance ammeter (Model HP 34401A). By convention, net anodic currents were assigned positive signs. To evaluate the individual impedance response of the two macrocell components in the galvanic couple, the components were disconnected and a battery-operated *dc* current source of impedance at least one order of magnitude above the impedance of each component of the couple was connected across the components, to preserve the individual static polarization conditions (Figure 2). The component to be tested was then connected to the EIS system as usual, and the other component of the couple remained *dc*-polarized but nearly free of *ac* excitation current during the EIS test.

RESULTS

In the following, experimental trends exemplified for single specimens were comparable to those observed in replicate specimens unless otherwise noted. No under-gasket crevice corrosion developed in any of the specimens for which results are reported [(1)].

Figures 3 and 4 exemplify the E_{OC} evolution as a function of exposure time for up to ~3,000 hr of the LCB and SCB specimens, respectively. In both P and NP solutions, E_{OC} values of the LCB specimens were ~-780 mV immediately after immersion, increasing to nearly constant values of ~-740 mV [(2)] for a period ranging from ~500 hr to ~1,700 hr of exposure. At the end of that stage, E_{OC} started a gradual decrease to attain terminal value of ~-920 mV for NP and P solutions, concurrent with the appearance of grayish discoloration of the aluminized surface around the perimeter of the exposed steel spot. The discoloration, moderate in P and darker in the NP system, later covered uniformly the entire aluminized surface forming an adherent layer ~10-15 μm (NP) and <1 μm (P) thick as measured by a magnetic thickness gauge after the end of the exposure. Further SEM-EDS analysis of a dried portion of that layer was consistent with the presence of aluminum hydroxide in agreement with the results reported elsewhere[13]. The SCB specimens exposed to P and NP showed E_{OC} values of ~-750 mV immediately after immersion, then decreased to ~-900 mV after a period ranging from ~50 hr to ~200 hr. During exposure, a grayish discoloration similar to that noted for the LCB specimens started at the aluminized surface in the vicinity of the exposed steel in NP solution, eventually covering uniformly the entire aluminized surface and forming an adherent layer ~5-10 μm thick. The appearance of initial discoloration however was not concurrent with the beginning of the E_{OC} drop but instead was noted after ~1,000 hr of exposure. In contrast, the aluminized surface of the SCB specimens exposed to solution P did not show discoloration or pits throughout the entire test period. In solution SW, both LCB and SCB specimens showed E_{OC} values ~-750 mV a very few hrs after immersion followed by a sharp decrease to ~-880 mV, not coincident with the appearance of light aluminized surface discoloration which took place after ~275 hr. The SCB specimens exposed to solution C showed E_{OC} values of ~-620 mV a few hrs after immersion followed by a gradual drop to ~-810 mV after ~1,000 hr, and then recovered slowly reaching ~-710 mV by the end of exposure. The appearance of dark discoloration in C was coincident with the E_{OC} decay.

A few hrs after immersion, visual examination conducted on the exposed steel of the LCB and SCB specimens exposed to solutions P and NP already showed a uniform reddish/black scale (likely rich in Fe^{+2}/Fe^{+3}) formed over the entire steel surface. Later on, the scale in those specimens grew until forming a rust layer ~300 μm thick. At ~450 hr of exposure, the central ~0.3 cm^2 of the exposed steel area of all LCB specimens in both solutions had a 1-3 mm thick porous reddish growth. There was noticeable additional steel metal loss underneath the central growth in the LCB specimens in NP, but less so in P. No such central growth was observed in the SCB specimens exposed to those solutions. At ~500 hr, small crystals appeared on top of the Fe-rich scale in both LCB and SCB specimens immersed in solution P. SEM-EDS

---

(1) Results for the LCB specimens exposed to solution C and for the macrocell assemblies in solutions C and SW are not available because significant crevice corrosion developed underneath the sealing gasket.

(2) Values of E_{OC} obtained with a Luggin probe, placed at various radial locations of the LCB specimens in solutions P and NP at ~72 hr and at ~200 hr of exposure, were only ~1-2 mV more positive over the exposed steel than over the unblemished aluminized coating surface.

compositional analysis of few crystals obtained from the LCB specimens in P was consistent with the presence of $CaCO_3$. During post-exposure cleaning, the scales on the exposed steel in solution NP were easily removed, but were more adherent in solution P. The exposed steel of the SCB specimens in solution C showed corrosion in only one of the triplicate specimens, an early formation of a thin reddish scale (likely rich in Fe^{+2}) that later developed to form a layer ~<300 μm thick on top of the steel. The exposed steel of the SCB specimens in SW was bright and free of corrosion scales throughout the entire exposure, and there was only very light steel discoloration with no corrosion deposits of the LCB specimens.

Post exposure evaluation showed that corrosion damage associated with uniform discoloration appeared to be mainly associated with changes in the outer aluminized coating layer, as confirmed by metallographic examination, and only with few visible small accompanying pits. Some of those pits, however, appeared to have reached the base steel as red rust deposits were noted at the pit mouths. Interestingly, metallographic examination conducted on cross sections near the aluminized/exposed steel edge of the LCB and SCB specimens in NP and C solutions showed an annulus ~50-70 μm wide surrounding the exposed steel spot of severe corrosion, not noted in any of the specimens in solutions P and SW. As a result, the outer aluminized coating layer was completely consumed, exposing the inner layer which appeared to remain intact for the time frame examined.

Immediately after immersion, bulk pH values were ~7.5 for all solutions. As time progressed, the bulk pH for solutions P and SW steadily increased to reach ~8.0 for both LCB and SCB configurations, respectively. The bulk pH for solution NP showed an increase to terminal pH values of ~9.0 (SCB) after only ~200 hr and ~8.8 (LCB) near the end of the exposure. In solution C, the bulk pH showed pH fluctuations (around a pH unit) around the terminal pH of ~7.5. Comparable pH trends were also observed for the macrocell assemblies exposed to solutions NP and P. The Fe^{+2} content in all solutions tested, measured by Atomic Absorption Spectroscopy after ~2,000 hr, was <0.01 ppm.

Figure 5 exemplifies the EIS results for the LCB specimens in solutions NP and P, for the period before and after the onset of the E_{OC} drop. For the period before the onset of the E_{OC} drop, the 1 mHz impedance moduli in both solutions were small (~<1.5 kΩ for NP and P). Per visual assessment of the specimen surface, the impedance behavior during that period was expected to be dominated mainly by the impedance of the steel portion by itself since corrosion scales there were notable, indicative of significant corrosion rates and correspondingly large integrated admittance. In contrast, the aluminized surface remained bright, suggesting passive behavior with consequent very small integrated admittance despite the large aluminized surface. After the onset of the E_{OC} drop, the 1 mHz impedance moduli decreased even further to ~150 Ω (NP) and ~250 Ω (P), consistent with active corrosion of the aluminized surface in both solutions. At that stage, the impedance behavior was expected to be dominated mainly by the impedance of the uniformly corroding aluminized portion, whereas the exposed steel was cathodically protected by the surrounding aluminized surface as demonstrated below. The EIS results for solution SW (Figure 5) show that the 1 mHz impedance moduli ranged from ~2.5 kΩ to ~4.5 kΩ throughout the test, expected to be dominated by localized corrosion of the large aluminized portion. As before, the exposed steel was cathodically protected by the surrounding aluminized surface as discussed later. The EIS results for the SCB specimens (data to be shown in subsequent paper) showed that in all cases, the EIS behavior was expected to be dominated mainly by the impedance of the active

(NP, SW, and C systems) and passive (P system) aluminized surface. The exposed steel in all cases remained cathodically protected so its impedance was expected to be comparably large to that of the aluminized coating.

The EIS response of the macrocell assemblies before and after the onset of the low E_{OC} regime is shown in Figures 6 and 7. Before the E_{OC} drop, the 1 mHz impedance moduli of the aluminized component were large (~55 kΩ for P and ~13 kΩ for NP), consistent with generally passive behavior and absence of visual evidence of active corrosion. The 1 mHz impedance modulus for the steel component was ~1 kΩ for both solutions, consistent with the observation of early corrosion deposit formation on the steel surface in both environments. Notably, the overall EIS response of the coupled assemblies in both solutions nearly equaled that of the steel component by itself, indicating that the steel ruled the EIS behavior of the macrocell coupled system. The EIS diagrams before the E_{OC} drop were usually describable by two overlapping loops, both approaching ideal capacitive behavior for the aluminized component, and deviating from ideal behavior for the steel component. After the E_{OC} drop, the 1 mHz impedance moduli of the aluminized component in both solutions greatly decreased to ~1-2 kΩ, consistent with the appearance of uniform discoloration and light pitting indicative of ongoing corrosion. In addition, the EIS diagrams of the steel component in both solutions resembled a nearly straight line rather than the earlier depressed semicircular appearance. The 1 mHz impedance magnitudes of the coupled assemblies nearly matched those of the aluminized component by itself, indicating that the aluminized coating dominated the impedance behavior of the coupled system during the low E_{OC} regime.

Figure 8 illustrates the E_{OC} and galvanic current (I_{galv}) evolution for the unblemished aluminized steel/exposed steel coupled assemblies in solutions P and NP. In both solutions, the unblemished aluminized steel component of the couple was always a net anode while the steel component was a net cathode. The combined E_{OC} trends, rust evolution at the exposed steel, and changes in the appearance of the unblemished aluminized coating generally paralleled those of the LCB specimens reported above. The early I_{galv} values were ~14 μA and ~1.5 μA for solutions NP and P, respectively. Upon the later E_{OC} drop, I_{galv} in both solutions showed corresponding increases toward terminal values of ~60 μA for NP and ~35 μA for P.

DISCUSSION

The E_{OC} trends and appearance of aluminized surface discoloration of the LCB specimens in solutions NP and P were consistent with the macrocell galvanic current trends recorded for the coupled macrocell assemblies exposed to the same solutions. Measurements of galvanic currents demonstrated that the outer aluminized coating layer behaved always as net anode upon contact with steel. However, the amount of macrocell current delivered by the outer coating layer in those solutions was insufficient to prevent rust formation on the steel surface early on in the exposure. This weak early galvanic action could be attributed to a predominantly passive condition of the outer aluminized coating layer, as manifested by its large impedance moduli in both solutions early on. Larger galvanic currents were expected in both solutions upon signs of corrosion of the outer aluminized coating later on in the test. There were no macrocell current measurements available for the SCB specimens exposed to solutions P and NP but uniform corrosion scales were noted on the steel surface, indicative of insufficient galvanic protection by the surrounding aluminized coating early on in the exposure. In contrast, the steel portion of the SCB and LCB specimens in solution SW showed none to

very light discoloration over the entire exposure time. Those results indicate strong galvanic protection by the surrounding aluminized coating in SW solution, consistent with observation of pitting of the aluminized surface and some secondary macroscopically uniform corrosion. Protective regime was established soon, as manifested by the drop of E_{OC} into protective potentials after only about two days of exposure for both LCB and SCB specimens in solution SW. The galvanic behavior of the SCB specimens in solution C showed variability, in that one of three specimens showed signs of steel corrosion but in all cases an annulus of aluminized outer layer corrosion wastage around the steel was noted. It is intriguing, however, that the relatively positive E_{OC} (~-620 mV) in all replicate specimens existed for at least ~1 hr up to ~100 hr and clearly protective potentials did not develop until about ~600 hr, yet the steel showed no signs of corrosion in two cases. For those cases, however, it should be recalled that severe aluminized corrosion was limited to the aforementioned annulus of pronounced coating loss around the steel. With such tight macrocell configuration, the local steel potential could have been significantly more negative than that measured by the reference electrode several diameters away, so the recorded E_{OC} values may have be misleading.

In the LCB specimens exposed to solution P, the most striking feature was that after an interval of time the aluminized surface experienced macroscopically uniform activation and the potential dropped dramatically, with the aluminized surface acting as a strong protecting anode to the exposed steel. The activation of the aluminized surface was manifested by light gray discoloration and the appearance of a few small macroscopically apparent pits [(3)]. It is tentatively proposed that the macroscopically uniform corrosion reflects the combined presence of many micro pits distributed on a spatial scale comparable to that of the inclusions plus some alkaline dissolution[16] as well, but likely to be of secondary importance because of the relatively large buffering capacity of solution P. The discoloration of the aluminized surface can be viewed as the result of precipitation of hydrated alumina outside the mouths of those pits. The large cathodic current at the exposed steel plus additional cathodic action at inclusions (minus the current needed to balance any alkaline dissolution) sustains the combined anodic processes at the micro pits.

For both SCB and LCB configurations in solution NP, there was also delayed onset of macroscopically uniform active corrosion. Some of the processes proposed above are likely to be present here too, with the important difference that this solution evolves spontaneously with time to increasingly higher bulk pH values (~9.0) as result of interaction with open air. The onset of the high corrosion regime then appears to be associated with the pH increase, and alkaline oxidation[16] is probably the dominant form of deterioration, aggravated by the coupling with the strongly cathodic steel surface. Consistent with this interpretation, in both LCB and SCB specimens in NP there was severe aluminized surface corrosion (with complete consumption of the outer coating layer) immediately around the perimeter of the exposed steel region as expected from the local increase in pH from O_2 reduction at the rim of the exposed steel. While macroscopically uniform, the corrosion of the aluminized surface may have been more localized at the microscopic level, likely involving aluminum surrounding inclusions, where increasingly higher pH takes place because of O_2 reduction, or because of some extent of micro pit formation around those inclusions following the initial alkaline oxidation

[(3)] The macro pits are deemed to be inconsequential because of their small number and dimensions, and their consequently large combined associated ohmic resistance, which would yield only a small fraction of the observed macrocell current.

undercutting. Solution NP has significant buffering strength, but the effects of local alkalinization around inclusions may be still important because they would be additional to that of the already enhanced high bulk pH of the solution. Macro pits were few in these systems and appear to be secondary per the arguments exposed earlier.

In solution C, only SCB specimens were evaluated. Unlike the other solutions, solution C has negligible buffering power and the effects of local alkalinization at inclusions are likely to be important. The bulk solution pH remained nearly neutral, so widespread alkaline oxidation as proposed for solution NP does not appear to be the main cause of the observed discoloration. Instead, localized alkalinization may have been responsible for generation of finely dispersed micro pits at the inclusion size scale, which would then represent the main form of aluminum attack. Such mechanism is subject to the same caveats noted above for the case of solution P. In solution C, however, the initiation of micro pits is facilitated by the lower buffering capacity, which may explain why activation took place even though the coating break was small. In the case of solution SW, where surface discoloration was light, the presence of a few macro pits, likely nucleated around inclusions, was notable. This condition can be explained by the strong aluminum pitting tendency in highly concentrated chloride solutions as in the solution SW (~20,000 ppm chloride concentration as opposed to only ~370 ppm in the other media used in this work). Thus, in the SW medium anodic action on the aluminized surface was likely limited to the active pits and the observed light discoloration indicated only secondary global distress in the form of vestigial alkaline oxidation.

The following interpretation of the EIS response addresses the coupled assemblies in solutions P and NP consistent with the above speculations. The EIS data of the blemished specimens were similarly analyzed and the results were comparable with those of the coupled assemblies. Figure 9 shows the analog circuit chosen to simulate the EIS response. R_S represents the effective solution resistance. It is assumed that the overall interfacial admittance can be divided into two branches. The lower branch is for the aluminized component and describes scenarios for both before and after active corrosion of the outer aluminized coating layer as described by Caseres[14]. The upper branch is for the exposed steel and describes scenarios for both before and after the E_{OC} drop. For the period before the E_{OC} drop, the circuit consists of a polarization admittance given by:

$$R_{a1}^{-1} = 2.3\, i_{a1}/\beta_{a1} \qquad (1)$$

where i_{a1} is the anodic current density and β_{a1} is the anodic Tafel slope for the activation polarization of the anodic reaction ($Fe \rightarrow Fe^{+2}+2e$) in parallel with a Constant Phase Angle Element CPE_1 representing the interfacial charge storage at the steel surface, and an admittance given by a series combination of a diffusional component W_1 governed by activation/concentration polarization of the cathodic reaction and a polarization admittance of the form:

$$R_{C1}^{-1} = 2.3\, i_{C1}/\beta_{C1} \qquad (2)$$

where i_{C1} is the cathodic current density and β_{C1} is the cathodic Tafel slope. The cathodic reaction is likely to be $O_2+2H_2O+4e \rightarrow 4OH^-$ and, for simplicity, to occur under simple one-dimensional conditions. After the E_{OC} drop, the exposed steel is polarized down to potential levels where the Fe/Fe^{+2} reaction is near equilibrium[17]. The corresponding equilibrium current

density is expected to be small with correspondingly small admittance. The remaining reaction of importance is expected to be O_2 reduction, occurring at a diffusion-limited, potential-independent value.

The analog circuit yielded good best-fit simulations of the EIS responses, shown by the solid lines in Figures 6 and 7. The nominal corrosion rates of the exposed steel i_{corrFE} were roughly estimated using the Stern-Geary relationship[19]:

$$i_{corrFE} \sim \beta_{a1}\beta_{C1}[2.3\ (\beta_{a1}+\beta_{C1})]^{-1}\ (A_{FE}\ R_{CT})^{-1} \quad (3)$$

where A_{FE} is the nominal steel area and R_{CT} is the charge transfer resistance of the form:

$$R_{CT} = [R_{a1}^{-1} + R_{C1}^{-1}]^{-1} \quad (4)$$

for the assumed values of β_{a1}=60 mV/dec and β_{C1}=120 mV/dec[18].

For the period before the E_{OC} drop, i_{corrFE} values were large (~250 μm/y) for NP and smaller but still considerable (~150 μm/y) for P, in keeping with the observation of corrosion deposits over the steel surface in both solutions. After the E_{OC} drop, i_{corrFE} values were smaller ~27 μm/y for P and ~32 μm/y for NP by the end of exposure, in agreement with the observation of terminal E_{OC} that approached that of the Fe/Fe^{+2} equilibrium reaction. The nominal corrosion rate i_{corrAL} of the aluminized component before the E_{OC} drop was roughly estimated by assuming that the anodic reaction was nearly potential-independent:

$$i_{corrAL} \sim \beta_{C2}\,(2.3\ R_{AL1}\ A_{AL})^{-1} \quad (5)$$

where A_{AL} is the nominal unblemished aluminized surface area. Values of i_{corrAL} were small (~0.7 μm/y) for P and higher but modest (~2 μm/y) for NP. For conditions after the E_{OC} drop, the i_{corrAL} was calculated using the value of R_{AL2} and considering for simplicity that both anodic and cathodic reaction polarizability have the same anodic and cathodic Tafel slopes assumed to be $\beta_{a2}=\beta_{C2}$=200 mV/dec. Thus[20]:

$$i_{corrAL} \sim 0.5\ \beta_{C2}\,(2.3\ R_{AL2}\ A_{AL})^{-1} \quad (6)$$

The resulting i_{corrAL} values were modest (~3.8 μm/y) for P and larger (~44.5 μm/y) for NP. It is noted that if the magnitude of i_{corrAL} were sustained, it would mean complete penetration of the outer aluminized layer in <1 yr of service. In a previous investigation[12], it was reported that unblemished aluminized steel had extremely low corrosion rates (~0.07 μm/y) after 3,000 hr of exposure to solution P and higher but still modest corrosion rates (~3.8 μm/y) in NP solution. These values were consistent with the visual observation of corrosion-free aluminized steel surface for the P solution and very slight discoloration for NP by the end of the exposure period. However, the presence of coating breaks exposing underlying steel caused corrosion damage of the aluminized coating as early as after 500 hr of exposure. Thus, coating breaks in aluminized steel do appear to be adverse for the time frame examined.

CONCLUSIONS

1. Galvanic protection was eventually provided by the surrounding aluminized surface to the base steel exposed at coating breaks in all the environments tested. However, in the less aggressive media (e.g. the solution P), protection developed only after some corrosion of the base steel had already taken place. The unprotected regime was as long as thousands of hours, during which the open circuit potential was comparable to that of steel by itself.

2. At the end of that positive potential trend period, blemished aluminized surface (except for the specimens with small coating break in solution P) showed signs of developing a macroscopically uniform active condition. The open circuit potentials at that stage were ruled by the aluminized coating.

3. The mechanism of activation of the aluminized layer may involve local alkalinization from enhanced cathodic reaction at the inclusions (especially in the low buffering capacity solution C), which would activate aluminum in the form of micro pits at the scale of the finely distributed inclusions present in the outer aluminized coating layer. Alkalinization may have been greater next to the steel region due to faster O_2 reduction rates there, consistent with the observation of a discoloration front radiating from the central exposed steel area.

ACKNOWLEDGEMENTS

This investigation was supported by the Florida Department of Transportation and the Federal Highway Administration. Special thanks to Mersedeh Akhoondan for conducting valuable experimental work. The opinions and findings described here are those of the authors and not necessarily those of the funding agencies. The authors are indebted to Contech Construction Products Inc. for providing the test material.

REFERENCES

1. J.O. Park, C.H. Paik, Y.H. Huang, R.C. Alkire, "Influence of Fe-Rich Intermetallic Inclusions on Pit Initiation on Aluminum Alloys in Aerated NaCl", Journal of Electrochemical Society 146 (1999), pp. 517-523

2. K. Nisancioglu, "Electrochemical Behavior of Aluminum‐Base Intermetallics Containing Iron", Journal of Electrochemical Society 137 (1990), pp. 69-77

3. K. Nisancioglu, K.Y. Davanger, O. Strandmyr, H. Holtan, "Cathodic Behavior of Impure Aluminum in Aqueous Media", Journal of Electrochemical Society 128 (1981), pp. 1523-1526

4. A.A. Sagüés, "Corrosion Measurement of Aluminum Alloys and Reinforced Concrete for Determination of Culvert Service Life", Final Report No. 99700-7324, FL Department of Transportation (1989)

5. R.A. Legault, V.P. Pearson, "Kinetics of the Atmospheric Corrosion of Aluminized Steel", Corrosion 34 (1978), pp. 344-348

6. H.E. Townsend, J.C. Zoccola, "Atmospheric Corrosion Resistance of 55% Al–Zn Coated Sheet Steel: 13 Year Test Results", Materials Performance 18 (1979), pp. 13-20

7. H.E. Townsend, A.R. Borzillo, "Twenty-Year Atmospheric Corrosion Tests of Hot-dip Coated Sheet Steel", Materials Performance 26 (1987), pp. 37-41

8. J. Creus, H. Mazille, H. Idrissi, "Porosity Evaluation of Protective Coatings Electrodeposited on Steel", Surface and Coatings Technology 130 (2000), pp. 224-232

9. B.A. Shaw, P.J. Moran, "Characteristics of the Behavior of Zinc-Aluminum Thermal Spray Coatings", Materials Performance 24 (1985), pp. 22-31

10. W. Li, S. Liu, Q. Huang, M. Gu, "Hot Dipped Aluminising (HDA) of a Low Carbon Steel Wire", Materials Science and Technology 19 (2003), pp. 1025-1028

11. ASM Metals Handbook, Vol. 7: Atlas of Microstructures of Industrial Alloys, 8^{th} Ed. Metals Park, OH, (1972) p.12

12. L. Caseres, A.A. Sagüés, "Corrosion of Aluminized Steel in Scale-Forming Waters", CORROSION/05, paper no. 05348 (Houston, TX: NACE, 2005)

13. J.R. Davis, "Corrosion of Aluminum and Aluminum Alloys", ASM International Materials Park, OH (1999)

14. L. Caseres, "Electrochemical Behavior of Aluminized Steel Type 2 in Scale-Forming Waters", Ph.D. Dissertation, University of South Florida (2007)

15. M.B. Vukmirovic, N. Dimitrov, K. Sieradzki, "Dealloying and Corrosion of Al Alloy 2024-T3", Journal of Electrochemical Society 149 (2002), pp. B428-B439

16. S.-I Pyun, S.-M Moon, S.-H Ahn, S.-S Kim, "Effects of Cl^-, NO_3^- and SO_4^{-2} Ions on Anodic Dissolution of Pure Aluminum in Alkaline Solution", Corrosion Science 41 (1999), pp. 653-667

17. M. Pourbaix, "Atlas of Electrochemical Equilibria in Aqueous Solutions", NACE (1974), p. 389

18. H. Kaesche, in Metallic Corrosion, pp. 166, National Association of Corrosion Engineers (1985), Houston

19. M. Stern, A.L. Geary, "Electrochemical Polarization, I. A Theoretical Analysis", Journal of Electrochemical Society 104 (1957), pp. 56

20. W.J. Lorenz, F. Mansfeld, "Determination of Corrosion Rates by Electrochemical DC and AC Methods", Corrosion Science 21 (1981), pp. 647-672

TABLE 1
Chemical composition of steel substrate (% weight)

C	Mn	P	S	Si	Cu	Al	Cb	Ni	Cr	Ti	N	Mo	Fe
0.05	0.20	0.006	0.012	0.01	0.031	0.041	0.002	0.017	0.028	0.002	0.0036	0.003	Bal.

Mill test report provided by Contech Construction Products Inc.

TABLE 2
Synthetic solutions composition and properties

Solution	TA	TH	pH	Ca^{+2}, mg/L	Cl^{-}, mg/L	σ, µmho/cm
C (control)	6	2	~7.4	0	372	1,140
NP (non precipitating)	480	2	~7.8	0		1,850
P (precipitating)	184	52	~7.4	200		1,390
SW (precipitating - high chloride)	210	8,280	~7.3	419†	19,846†	40,000

TA=total alkalinity (mg/L $CaCO_3$), TH=total hardness (mg/L $CaCO_3$), σ=solution conductivity.
† Values reported by the manufacturer.

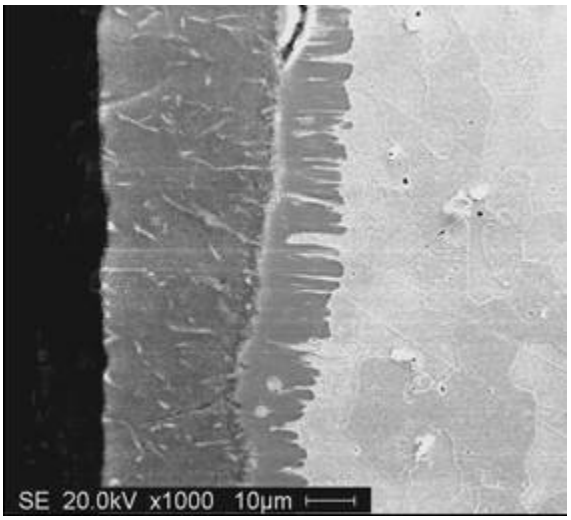

FIGURE 1 - Cross section (perpendicular to rolling direction) of a 1.59 mm thickness flat aluminized steel Type 2 specimen after etching with 2% Nital solution

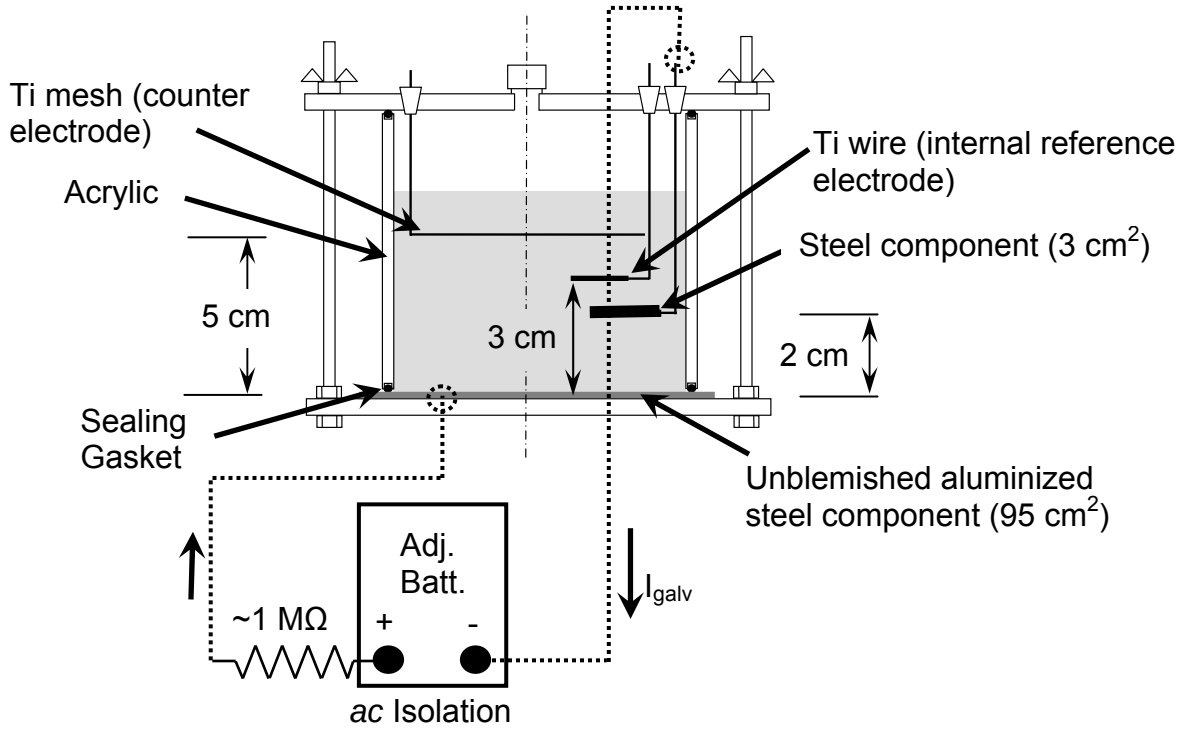

FIGURE 2 - Schematic of the test cell arrangement used to monitor galvanic currents and impedance behavior of the individual aluminized steel and steel components in the macrocell assemblies

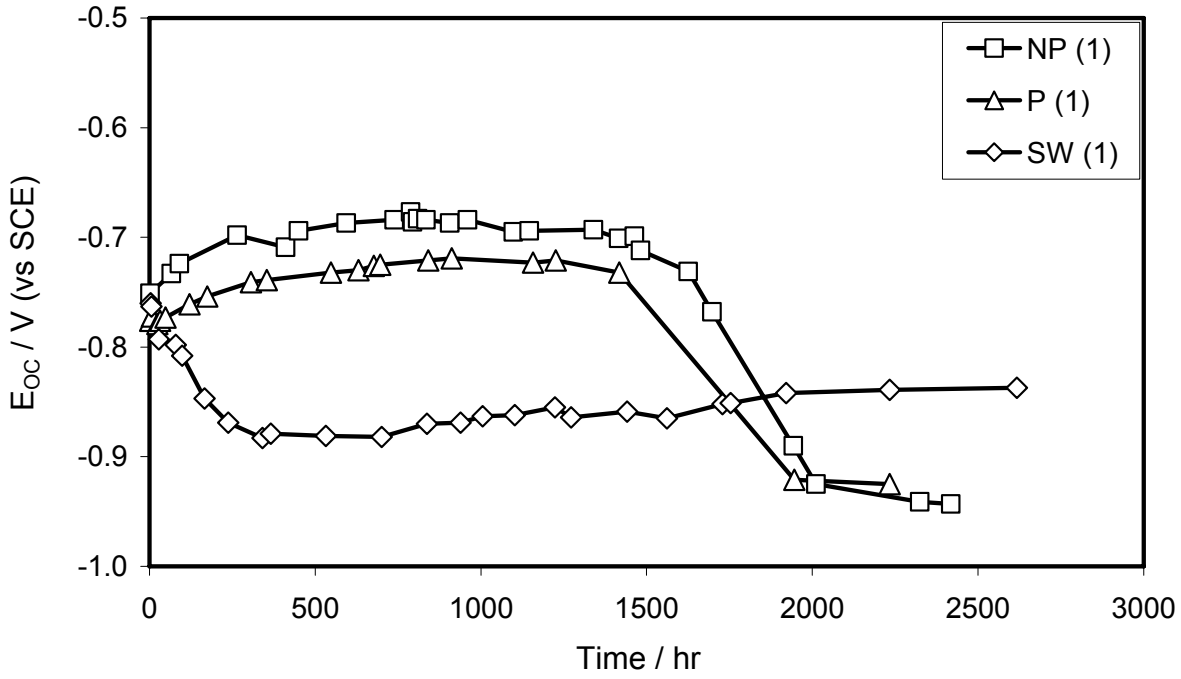

FIGURE 3 - E_{OC} evolution as a function of exposure time of the LCB specimens. Specimen number is denoted in parenthesis

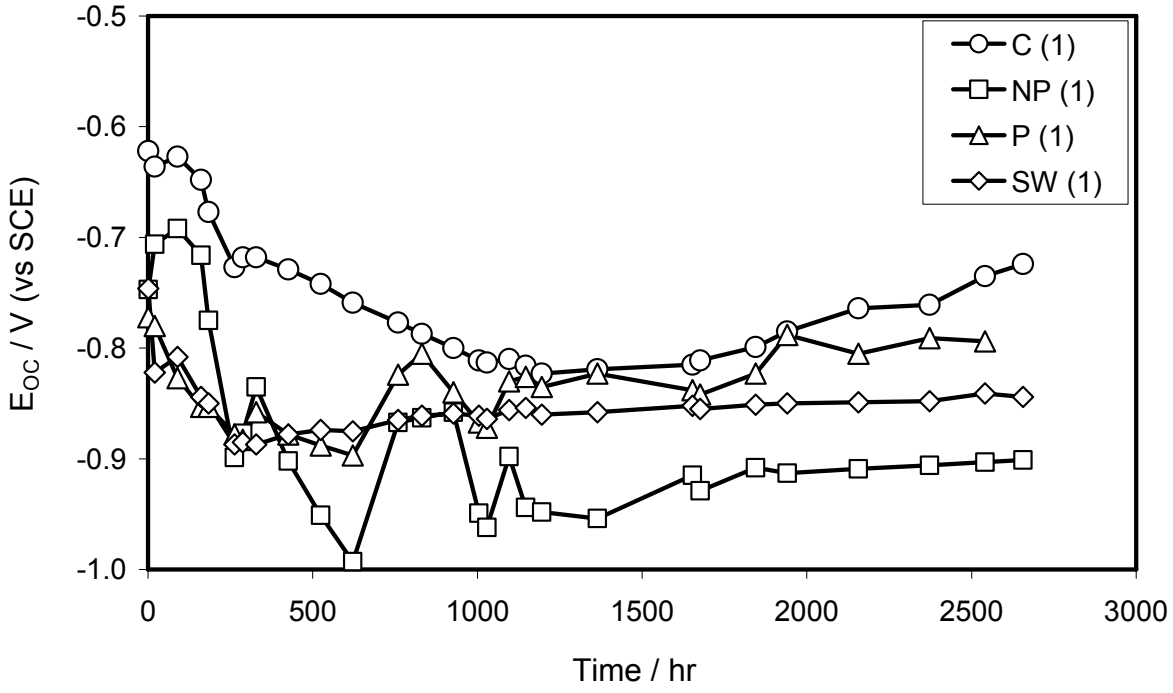

FIGURE 4 - E_{OC} evolution as a function of exposure time of the SCB specimens. Specimen number is denoted in parenthesis

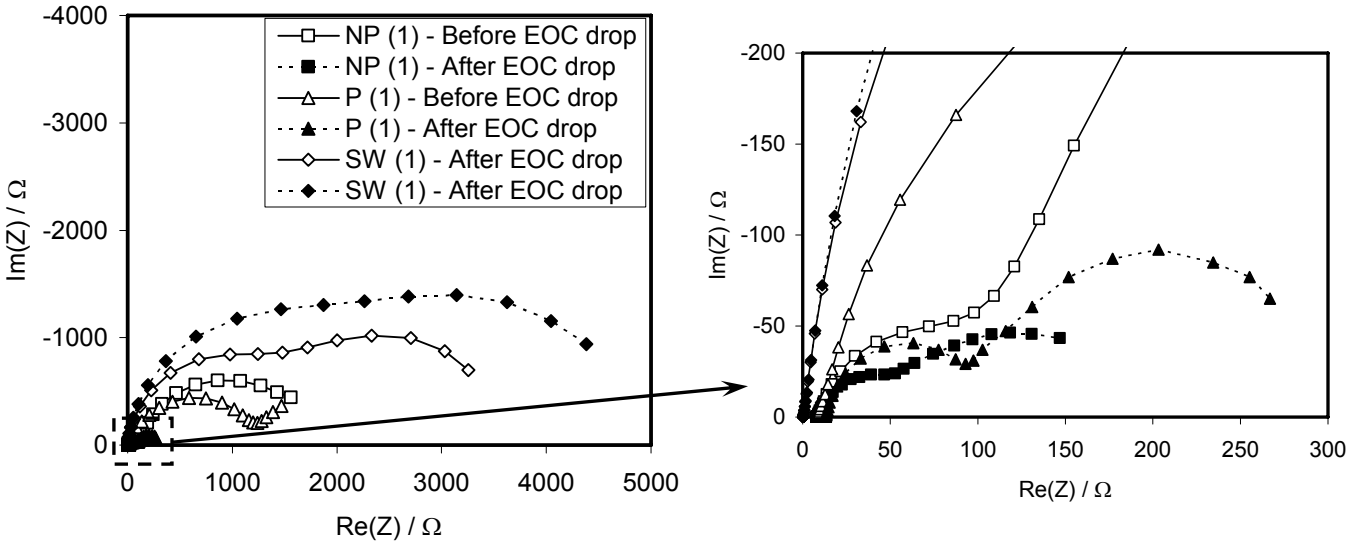

FIGURE 5 - EIS behavior response of the LCB specimens before and after the E_{OC} drop (100 KHz - 1 mHz - 5 points/dec). EIS measurements for solution SW were taken for the period after E_{OC} decay

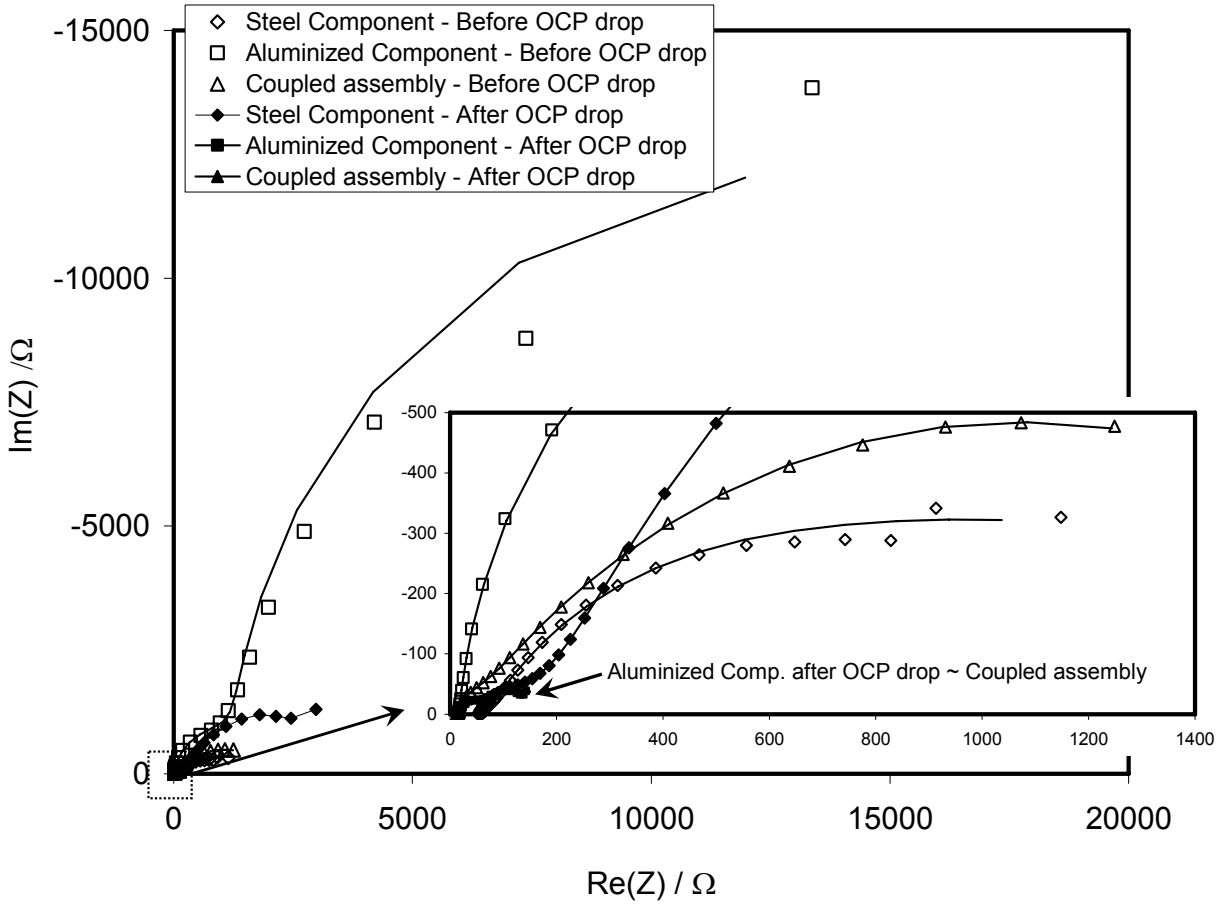

FIGURE 6 - EIS behavior of the interconnected aluminized steel/steel assembly (#1) and the individual components exposed to solution NP (100 kHz–1 mHz, 5 pts/dec) before (~900 hr) and after (~1,780 hr) E_{OC} drop

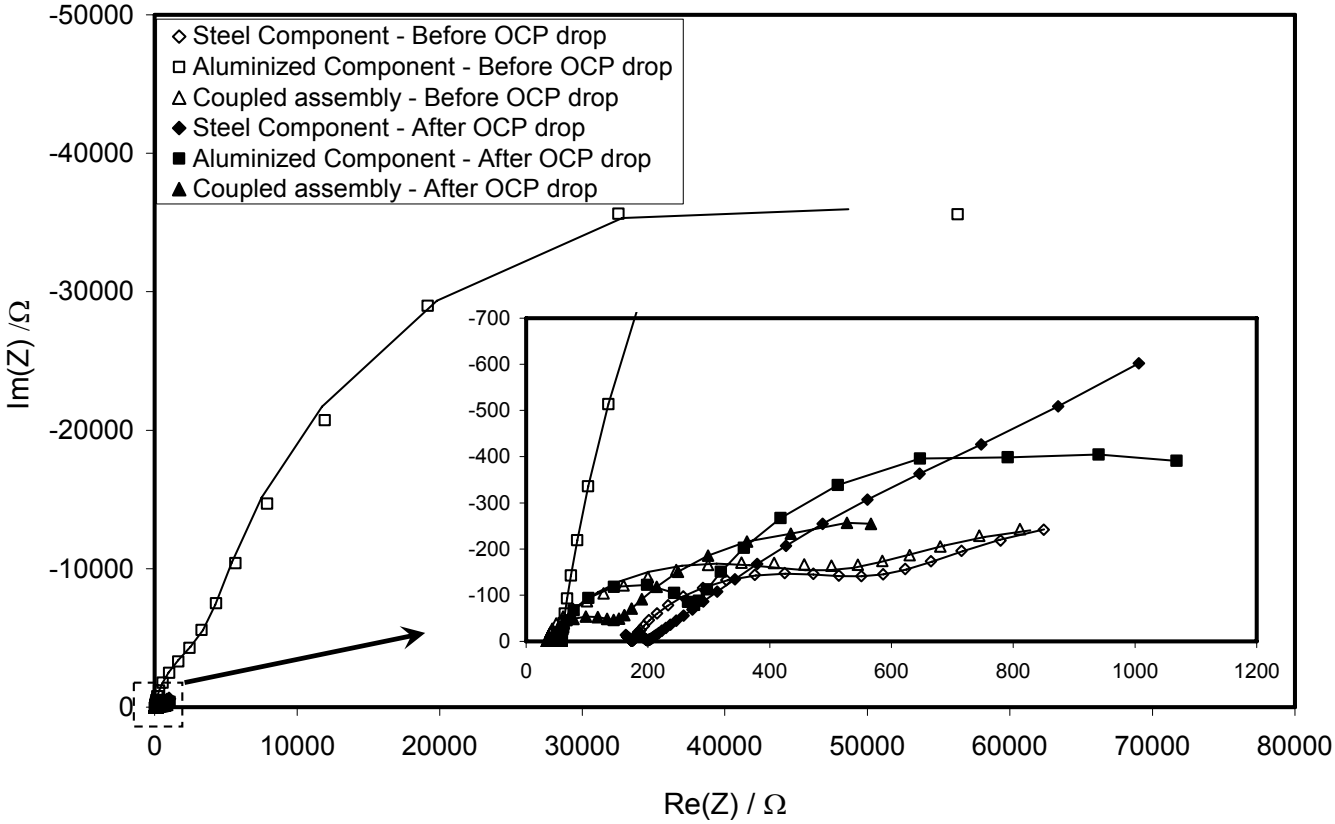

FIGURE 7 - EIS behavior of the interconnected aluminized steel/steel assembly (#1) and the individual components exposed to solution P (100 kHz–1 mHz, 5 pts/dec) before (~900 hr) and after (~1,780 hr) E_{OC} drop

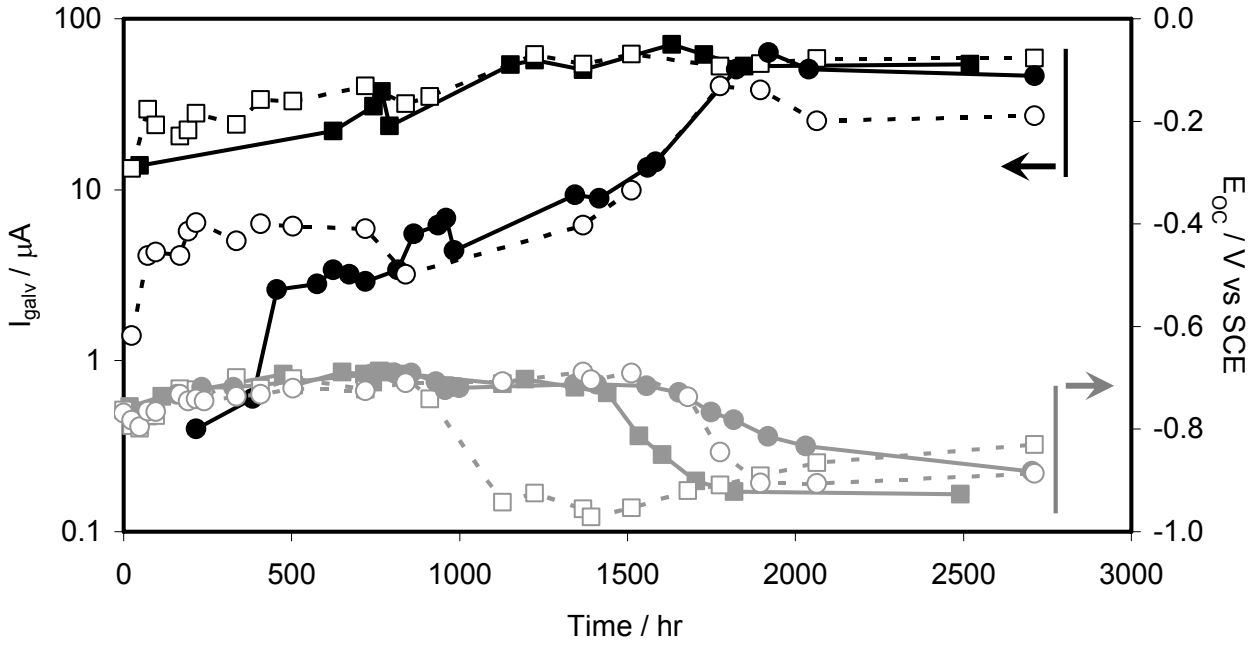

FIGURE 8 - E_{OC} and galvanic current I_{galv} measurements for the macrocell assemblies exposed to solutions P (circles) and NP (squares). Solid and dashed lines are for specimens #1 and #2, respectively. The steel components were always net cathodes

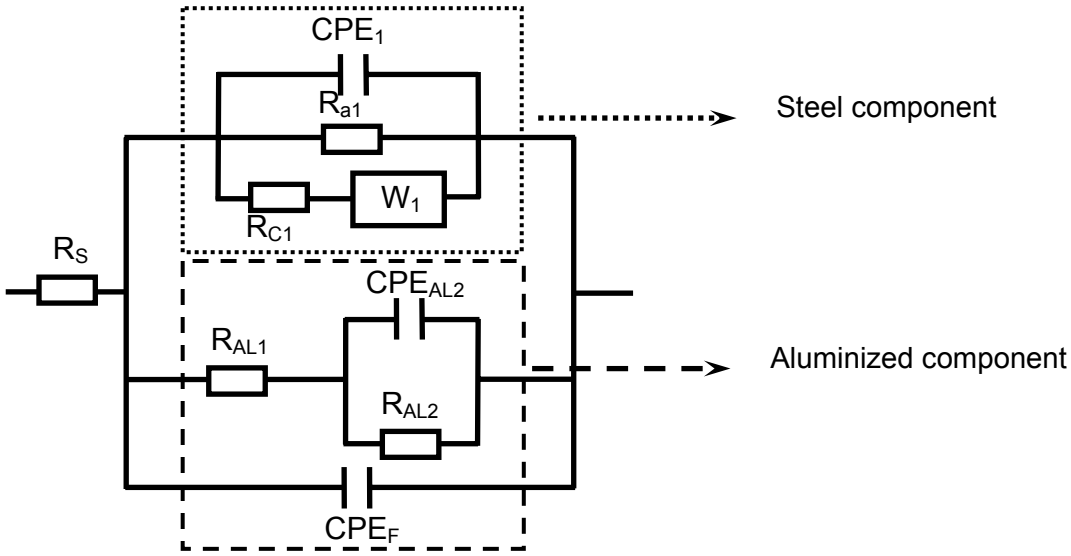

FIGURE 9 - Analog circuit used to simulate the impedance response of the macrocell assemblies in solutions NP and P for the regimes before and after the E_{OC} drop